Biological and Environmental Transformations of Copper-Based Nanomaterials

Zhongying Wang,[†] Annette von dem Bussche,[§] Pranita K. Kabadi,[§] Agnes B. Kane,[§,⊥] and Robert H. Hurt[‡,⊥,*]

[†]Department of Chemistry, [‡]School of Engineering, [§]Department of Pathology and Laboratory Medicine, and [⊥]Institute for Molecular and Nanoscale Innovation, Brown University, Providence, Rhode Island 02912, United States

ABSTRACT Copper-based nanoparticles are an important class of materials with applications as catalysts, conductive inks, and antimicrobial agents. Environmental and safety issues are particularly important for copper-based nanomaterials because of their potential large-scale use and their high redox activity and toxicity reported from *in vitro* studies. Elemental nanocopper oxidizes readily upon atmospheric exposure during storage and use, so copper oxides are highly relevant phases to consider in studies of environmental and health impacts. Here we show that copper oxide nanoparticles undergo profound chemical transformations under conditions relevant to living systems and the natural environment. Copper oxide nanoparticle (CuO-NP) dissolution occurs at lysosomal pH (4−5), but not at neutral pH in pure water. Despite the near-neutral pH of cell culture medium, CuO-NPs undergo significant dissolution in media over time scales relevant to toxicity testing because of ligand-assisted ion release, in which amino acid complexation is an important contributor. Electron paramagnetic resonance (EPR) spectroscopy shows that dissolved copper in association with CuO-NPs are the primary redox-active species. CuO-NPs also undergo sulfidation by a dissolution−reprecipitation mechanism, and the new sulfide surfaces act as catalysts for sulfide oxidation. Copper sulfide NPs are found to be much less cytotoxic than CuO-NPs, which is consistent with the very low solubility of CuS. Despite this low solubility of CuS, EPR studies show that sulfidated CuO continues to generate some ROS activity due to the release of free copper by H_2O_2 oxidation during the Fenton-chemistry-based EPR assay. While sulfidation can serve as a natural detoxification process for nanosilver and other chalcophile metals, our results suggest that sulfidation may not fully and permanently detoxify copper in biological or environmental compartments that contain reactive oxygen species.

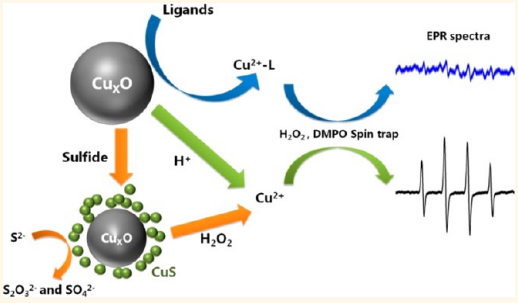

KEYWORDS: human health · environment · nanocopper · toxicity · redox activity · phase transformations

Copper-based nanomaterials are used in a range of established and emerging technologies that include catalysts, printable electronics, magnetic storage, solar energy conversion, wood protection, and antimicrobial products.[1−7] These uses will inevitably lead to human and environmental exposures that must be characterized and managed to ensure the safe development of copper-based nanotechnologies. In addition to engineered nanoparticles, copper also occurs as an "incidental" particle generated by chemomechanical polishing operations on copper-containing substrates in the semiconductor industry.[8] Copper-containing materials are widely used as antimicrobials and in agriculture as fungicides, algaecides, and herbicides. Relevant copper forms include carbonates, hydroxides, various oxide phases, and the zerovalent metal, and dissolution to bioavailable ions is a commonly assumed mode of activity. In other application fields, the most technologically important copper-based materials are zerovalent metal nanoparticles (Cu-NPs) and oxide nanoparticles, Cu_xO-NP, with $x = 1$ or 2. The potential for widespread exposure makes copper-based nanomaterials a high priority for risk characterization.

A second factor making nanocopper a high priority for study is its significant toxicity relative to other common nanomaterials.[9−16] Karlsson *et al.*[15] found that CuO nanoparticles were the most potent regarding DNA damage and cytotoxicity in a set of metal oxides and carbon nanotubes studied in parallel. Fahmy *et al.*[17] showed greater cytotoxicity of CuO nanoparticles in airway epithelial (HEp-2) cells relative to SiO_2 and Fe_2O_3 and demonstrated that oxidative stress was the cause of the

* Address correspondence to robert_hurt@brown.edu.

Received for review June 18, 2013 and accepted September 13, 2013.

Published online September 13, 2013
10.1021/nn403080y

cytotoxic effect. Studer *et al.*[14] attributed the cytotoxicity of CuO to its relatively high solubility in biological media and the impacts of dissolved copper ions, as also reported by Zhang *et al.*[9] There is a general consensus that toxicity in Cu/Cu_xO materials is due to oxidative pathways, but there is ongoing debate about the relative importance of ions and particle surfaces in primary ROS generation.[18]

It has become clear that nanomaterials can undergo chemical transformation in the environment or human body that profoundly influences their toxicity and risk.[19−24] This is especially important for metal-based nanomaterials, where the base metals themselves are indefinitely persistent but can occur in different compounds or phases that greatly affect metal bioavailability. Nanosilver, for example, is synthesized and sold in metallic form, but over its lifetime it can undergo oxidative dissolution, colloidal aggregation, sulfidation, and reaction with selenide with corresponding large changes in silver bioavailability and toxicity.[19,22,23,25−29] ZnO nanoparticles have been reported to partially dissolve in environmental and biological media and exert toxicity through the liberated zinc ions,[9,30,31] or to undergo sulfidation to the more stable ZnS.[32]

Several studies have examined transformations in copper-based systems.[10,33] In comparison to silver, metallic copper NPs oxidize more readily, first forming a Cu(I) oxide shell around a zerovalent core, and eventually to Cu(II) oxide as a final product.[10] Oxidation typically begins during fabrication and storage, so at the point of exposure or environmental release, an oxide or surface oxide is the most likely phase to come into contact with biological and environmental fluid phases.[10,34,35] For this reason, and because the oxidation process has already been systematically studied,[10] we chose to focus our study on the interactions of pre-existing copper oxide phases with biological and environmental systems.

There is significant evidence that dissolution is an important transformation in oxidized copper NPs.[9,10,13,14,33] Though generally regarded as "insoluble" substances, copper and copper oxide NPs appear to liberate sufficient amounts of soluble copper in relevant media to affect biological systems. Zhang *et al.*[9] measured the extent of dissolution of CuO in biological media and attributed cytotoxicity of CuO to the soluble fraction rather than particle surface reactions. Studer *et al.*[14] proposed a Trojan horse-type mechanism in which CuO nanoparticles penetrated the cell membrane followed by intracellular dissolution into redox active copper ions. Midander *et al.*[33] observed size-dependent ion release and toxicity when comparing nano- and micrometer-sized copper oxide particles. Free copper ions Cu^{x+} ($x = 1, 2$) are highly redox active species capable of producing hydroxyl radical by the following Fenton-like reaction:[36,37]

$$Cu(II) + H_2O_2 \rightleftarrows Cu(I) + {\bullet}HO_2 + H^+ \quad (1)$$

$$Cu(I) + H_2O_2 \rightarrow Cu(II) + OH^- + {\bullet}OH \quad (2)$$

so even small amounts of soluble copper can be biologically significant. On the basis of recent work on the dissolution in other NP systems, we hypothesize that pH, ionic strength, dissolved organic matter, and biomolecular ligands may play an important role in the toxicity of copper-based nanoparticles by influencing the total dissolved copper concentration.[38] This concentration, together with the relative redox activity of the ion and surface, should determine the origin of ROS generation and subsequent toxicity pathways in Cu-based nanomaterials, which are factors we hope to clarify in this study.

A final relevant transformation is reaction involving the earth-abundant element sulfur, which has been shown to be important for silver, zinc, and Cd nanomaterials[39] in both environmental[32,40−43] and biological settings.[22] Copper ions are soft (Cu^+) or borderline (Cu^{2+}) Lewis acids with high affinity for sulfide ligand, and form a highly insoluble sulfide phase, which suggests that copper oxides may undergo sulfidation to produce a material with low copper bioavailability. The synthesis literature shows that hollow CuS nanostructures can be synthesized using Cu_2O as sacrificial template,[44,45] but information on the natural bioenvironmental sulfidation pathways are limited. Sulfidation has been suggested as a natural detoxification process for metallic nanoparticles.[40,46,47]

The present study investigates the transformations of copper oxide nanoparticles in biological and environmental media, and their implications for copper bioavailability, redox activity, and toxicity. The results are directly relevant to CuO-based technologies and may provide qualitative insight into technologies based on metallic Cu or Cu(I) oxide materials that are capable of environmental oxidation to CuO or CuO outer corrosion films. We show that copper oxide undergoes not only acid-promoted dissolution, but also ligand-assisted dissolution in the presence of amino acids at neutral pH. Copper oxide also undergoes sulfidation to produce highly insoluble CuS nanoparticles. Surprisingly, sulfidation does not permanently suppress copper bioavailability and redox activity, because hydrogen peroxide at physiologically relevant concentrations oxidizes CuS and liberates free copper ions that partially restore redox activity in the form of OH, detected here by EPR methods.[36]

RESULTS AND DISCUSSION

Comparative Solubilities of Oxide and Sulfide Phases. Ion-particle partitioning is a major determinant of the fate, transport, and toxicity of nanoparticles, and understanding dissolution behavior has become an important theme in environmental nanotechnology and nanotoxicology research.[9,19,21,30,46,48−50] Figure 1 shows the equilibrium solubilities of oxide and sulfide phases for several metals found in the most common commercial nanomaterial types. Although based on bulk thermodynamic properties, this plot shows several trends that

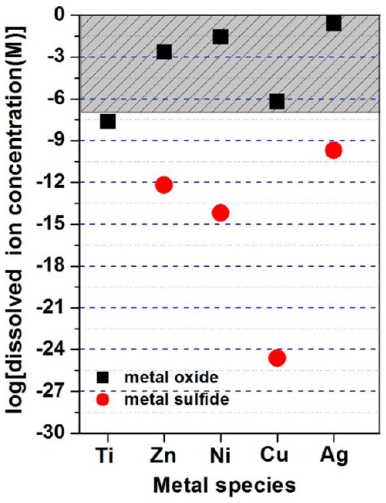

Figure 1. Equilibrium solubility of the oxide and sulfide forms of common metal-based nanoparticles. The equilibrium dissolved metal ion concentration was estimated using Visual MINTEQ 3.0 using bulk thermodynamic parameters (see Supporting Information for details). The phases considered were TiO_2, ZnO, NiO, CuO, and Ag_2O and the sulfides ZnS, NiS, CuS, and Ag_2S. The incubation conditions for the metal oxide calculations were aqueous solution (pH 7) and 1 mM $NaNO_3$ as electrolyte, and for metal sulfide ligand-free aqueous solution (pH 7) containing an environmentally relevant total sulfide concentration (1 mM). Please note the calculations ignore any oxidative dissolution. Toxicity studies on free ions typically show adverse biological effects at micromolar doses (>0.1 uM),[59−62] which defines the shaded region above. Data points that fall in the shaded region all correspond to cases where nanoparticle toxicity has been attributed to dissolution mechanisms (oxides of Zn, Ni, Cu, Ag), which is possible because of the finite solubility of the oxide phase. TiO_2 solubility in contrast is too low to yield ions above the micromolar range, where ion-induced toxicity is often seen in other systems.

provide insight into reported nanomaterial behavior. First, the most soluble oxides are those of Ag, Ni, and Zn, and all three have been reported to be toxic through dissolution mechanisms.[31,51,52] ZnO toxicity has been related to dissolution in several recent studies,[9,30,31] and NiO toxicity *in vitro* has been reported to correlate with the concentration of dissolved Ni^{2+} ion.[51] Silver oxidizes slowly and is typically synthesized and sold as the zerovalent metal, but it does dissolve upon use and disposal[46,49] through a mechanism that may pass through a Ag_2O surface intermediate.[53] Because the oxide has a relatively high solubility, the rate limiting step is typically the initial oxidation step.[54,55] Lower solubility oxides are titania, whose biological responses have not typically been related to dissolution, and copper, the subject of the present study.

Sulfide phases are typically much less soluble and have been reported to form when nanosilver is exposed to the natural environment[23,24,40−43,47] or biological fluid phases[22] and to reduce the toxicity relative to the original zerovalent form.[23,40,47,56] Sulfidation has been proposed as a natural detoxification mechanism for nanosilver[40,41,47] and potentially other chalcophile metals.[57,58] This is based on the fact that the equilibrium free metal in each of these sulfide systems is in the nanomolar range or below (Figure 1), which is well below typical threshold concentrations for biological effects. Copper(I) sulfide, CuS, is unique in its extremely low solubility (Figure 1), which led us to hypothesize that sulfidation would effectively detoxify nano-Cu or nano-CuO. We found here, however, that copper sulfides do form, but the redox activity of the product is not fully suppressed (*vida infra*).

Copper Ion Release in Biologically and Environmentally Relevant Media. Copper(II) oxide is described as insoluble in basic chemistry references, but at the ppm levels of interest in nanotoxicology and the environment, it is sufficiently soluble for the released ions to be key determinants of toxicity.[9,13,14] On the basis of eq 3, we expect CuO ion release to be pH dependent, and this is confirmed in Figure 2A. Solubility at lysosomal pH (4−5) is significant and can be close to complete at low particle loadings (Figure 2B), but at extracellular pH (7.4 in PBS buffer) it is very low. The very low ion release at pH 7.4 was initially surprising since copper ions have been reported to be the primary source of toxicity in several *in vitro* studies.[9,13,14] Calculations with Visual MINTEQ 3.0 at this pH confirm low values of dissolved copper ion (154 ppb) at equilibrium. These low values were further confirmed in time-resolved measurements (Figure S2A, Supporting Information), which gave copper concentrations about 20 ppb, which approached the detection limit of our inductively coupled plasma atomic emission spectroscopy (ICP-AES) technique.

$$CuO_{(s)} + 2H^{+}_{(aq)} \leftrightarrow Cu^{2+}_{(aq)} + H_2O_{(l)} \quad (3)$$

To understand how Cu ions exist in biological studies, we studied dissolution directly in two types of cell culture media (Figure 2C). We measured significant release in both media despite the high pH (7.4), suggesting dissolution is assisted by ligands, either thermodynamically by reducing the concentration of the free ion in equilibrium with the solid, and/or through kinetic effects at the particle surface. We tested a variety of single components found in cell culture media in an attempt to identify the primary types of ligands involved. Glucose and the buffering agent, HEPES, did not promote copper ion release, but fetal bovine serum (FBS) and glutamine did (Figure S2B, Supporting Information). Glutamine and other amino acids have been reported to form a high-affinity complex with copper, and the overall stability constant is very high (log β_2 of 11.6).[63] The removal of free ion shifts the ion-particle equilibrium and favors dissolution. The complex formation (stability) equilibrium constant, $K = [L - Cu^{2+}]/[Cu^{2+}][L]$, can be rearranged to give a dissolution enhancement factor as follows:

$$[\text{total copper}]/[\text{free ion}] = ([L - Cu^{2+}] + [Cu^{2+}])/[Cu^{2+}] = 1 + K[L] \quad (4)$$

which is 10^8-10^9 when the concentration of ligands (*e.g.*, glutamine) in cell culture media is in the mM range. We

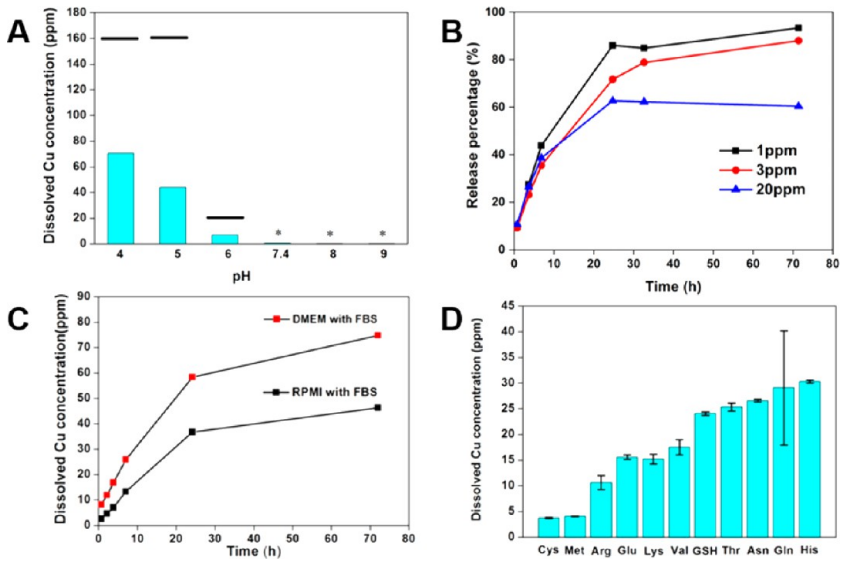

Figure 2. Dissolution behavior of CuO in various fluid media. (A) Soluble copper produced by 24 h incubation of CuO-NPs (initial concentration 200 ppm) as a function of pH (50 mM acetate buffers at pH 4, 5, and 6, PBS buffer at pH 7.4, and 50 mM borate buffers at pH 8 and 9). The black bars indicated the equilibrium concentration in the corresponding pH conditions calculated by Visual MINTEQ 3.0; the stars indicated that both the calculated equilibrium concentration and real dissolved Cu concentration is close to the ICP-AES detection limit (see Supporting Information for details). (B) Effect of initial CuO-NP loading on dissolution kinetics (acetate buffer at pH 4.9) for 3 days expressed as percent of total copper. Over 80% of CuO was dissolved after 30 h for 1 ppm initial loading of CuO-NPs and then dissolved Cu concentration slowly increased. (C) Soluble copper produced by 3-day incubation of CuO-NPs (initial concentration 200 ppm) in DMEM and RPMI cell culture media supplemented with 10% FBS at pH 7.4. Note the much elevated Cu ion release relative to PBS buffer at pH 7.4 (A). (D) Ligand effects on CuO (initial concentration 200 ppm) dissolution using a series of amino acids and the tripeptide glutathione at 2 mM in PBS buffer in 24 h. Please be noted that the dissolved copper measured is those that pass through the ultrafilters. Therefore, about cysteine, the dissolved copper concentration may be underestimated due to the formation of insoluble precipitate through copper−thiol bond.

further investigated the effects of a larger series of amino acids (Figure 2D), which all promoted dissolution, but to differing degrees. We thought this may be due to involvement of the side chain in complex formation, but previous studies have reported that only the amino and carboxylate terminal groups were involved.[64] Indeed the Cu^{2+} complexes with glutamine and histidine do not have higher stability constants than other amino acids, which also suggests their higher activity is not thermodynamic in origin. In the search for an alternative explanation, ligands have been reported to promote the dissolution of iron oxide through formation of surface complexes that kinetically enhance the detachment.[65] The surface binding constant for CuO-histidine is reported to be higher than that for other amino acids,[66] and the ion concentrations in Figure 2A are well below estimated equilibrium values (see horizontal bars). Both of these facts suggest the different activities among the amino acids are kinetics differences associated with ligand-specific surface binding ability.

ROS Production in Cu-NP Systems. Several studies of nano-Cu or nano-CuO toxicity report ROS generation and oxidative stress as a mechanism.[12,16,17] In copper-containing systems, ROS may be produced by heterogeneous reactions at the particle surfaces, or by dissolved copper, which can exhibit Fenton-like chemistry through the Cu(II)/Cu(I) redox couple.[12,67,68] Resolving the relative particle-ion contributions is key to understanding the mechanism of nano-Cu toxicity and interpreting nanotoxicology data. Studies showing correlation between dissolved Cu and toxicity suggest the primary redox species are in solution,[13] not on the surface, but direct evidence is needed. Here, we use EPR spin-trap techniques to quantify ROS production from particles, ions, and sulfidated products. We focus on the hydroxyl radical by using the spin trap DMPO, which is known to react with •OH to form an OH-DMPO adduct that exhibits a characteristic EPR peak quartet (see Figure 3). Incubation of CuO-NPs or copper ions with DMPO and peroxide in PBS buffer gives this characteristic EPR spectra, but with varying peak intensities as shown in Figure 3. Each of the copper-containing solutions triggers Fenton chemistry and produces the OH-DMPO adduct. Comparing the data on particles and their clear filtrates (Figure 3A) indicates that most of the activity in the CuO-NP cases is associated with the soluble fraction. Figure 2 predicts that this soluble fraction should be quite low under these conditions (<100 ppb), and indeed the "ion-only" experiments in Figure 3B show similar peak heights for 6−100 ppb free copper. Even at this limited degree of dissolution (neutral pH with no added ligands), the main source of ROS is the trace concentration of free copper ion.

We were interested in whether the ligands that promote Cu dissolution also affect redox activity in solution. Previous studies have shown that complex formation can reduce the catalytic ability of Cu ions in

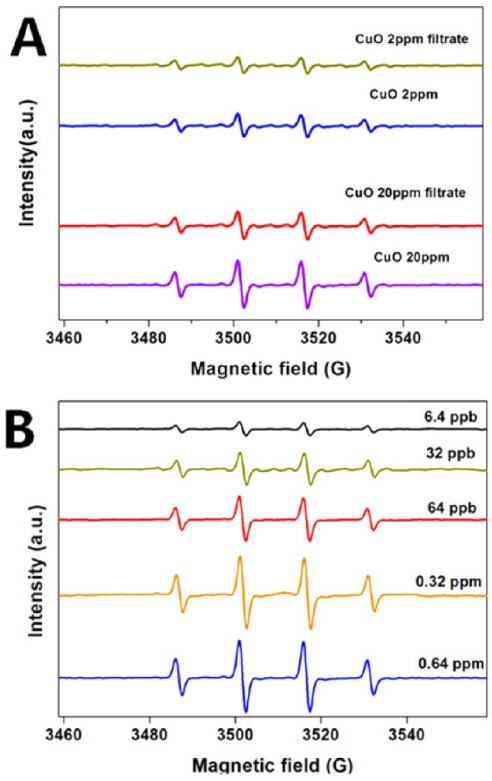

Figure 3. Hydroxyl radical EPR signal (DMPO spin trap) induced by (A) 2 or 20 ppm CuO-NPs suspension or its filtrate containing only the soluble forms, or (B) free copper ions ($CuCl_2$) at various concentrations (ppb ng of Cu/g of solution). These experiments used 1 mM hydrogen peroxide and 100 mM DMPO in PBS buffer for 20 min. To isolate the effect of the ion associated with the particles, CuO-NPs were incubated for 20 min in PBS buffer and then subjected to ultrafiltration, and the filtrate was added to 100 mM DMPO and 1 mM hydrogen peroxide in PBS for 20 min before the spectra were obtained ("filtrate" cases in A).

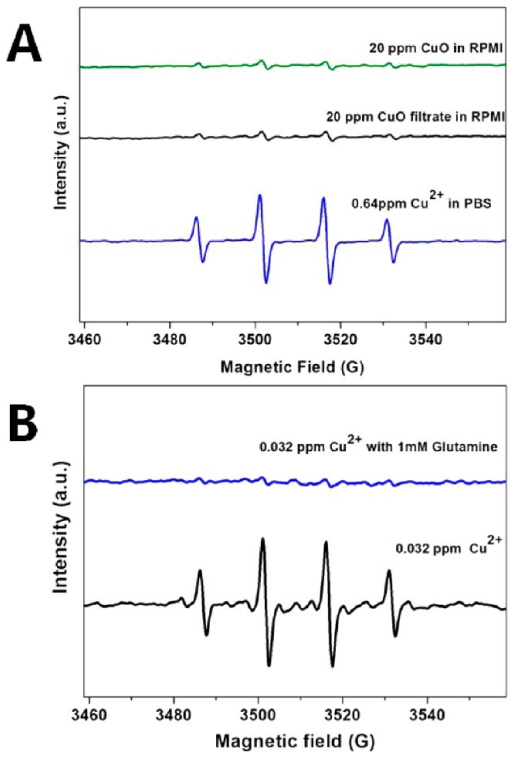

Figure 4. Ligand effects in the ROS activity of CuO-NPs and soluble salts. (A) Comparison of ROS activity of 20 ppm CuO-NPs or its filtrate in cell culture media with 0.64 ppm copper ions in PBS buffer. Note that the ion released from 20 ppm CuO-NPs in medium is much greater than the 0.64 ppm free ion concentration (Figure 2C), but is still less redox active because of ligand binding in medium. (B) ROS activity of 0.032 ppm Cu^{2+} with or without the presence of 1 mM glutamine in PBS buffer. Please be noted that the induced EPR peaks with glutamine were reduced but not eliminated and can increase with longer incubation time according to Figure S3 (Supporting Information).

peroxide reduction to •OH.[69] Figure 4 shows a strong attenuation of the •OH signal when simple PBS buffer (Figure 3) is replaced by cell culture medium (Figure 4A). Some redox activity remains in media (the OH-DMPO quartet is clearly visible) and is primarily associated with the soluble fraction, since the particles and their clear filtrates give similar peak heights (Figure 4A). The redox behavior is quite low in the presence of 1 mM glutamine (Figure 4B), which is a high affinity ligand (log β_2 of 11.6) and strong promoter of dissolution. The catalytic ROS production by Cu is significantly reduced in the media containing glutamine, but the complexed Cu can still catalyze the reaction though in a much slower manner (Figure S3, Supporting Information). Overall, the data in Figures 2–4 suggest that complex biological media will promote copper dissolution but then partially suppress the redox activity of the resulting soluble species. It is doubtful that simple assays for dissolution and redox activity in water or simple buffers will have predictive value for the toxicity of copper-containing NPs.

Copper Oxide Sulfidation. Recent research has shown that nanoparticles based on silver, zinc, and cadmium undergo reactions with reduced sulfur species (and in some cases selenium species)[22] in the environment and the human body to produce low-solubility metal sulfide (or selenide) phases. These transformations are expected to have profound effects on transport, bioavailability, toxicity, and risk.[22–24,32,40,46,47,57,70] Here we studied the reaction of CuO-NPs with soluble sulfide (main species is HS^-) as a function of time and CuO:sulfide stoichiometric ratios. Figure 5 shows conversion of CuO-NPs to sulfide phases within one day with the extent of conversion depending on the starting CuO:bisulfide molar ratio. At high sulfide (CuO:bisulfide = 1:5), the conversion is essentially complete as the XRD spectra lose all characteristic peaks for crystalline CuO and match quite well with Cu(I)S (covellite) reference spectra (Figure 5A). Though the formation of any Cu_2S phase was not observed, absence of a crystalline Cu_2S phase under these conditions may indicate a slow phase transition that prevents the crystalline phase from being observed over our time scales.[71] The morphologies of the sulfidated samples show a number of particles substantially smaller than the original CuO particles, and at least some of them in a crystalline state, indicated by HRTEM fringes (Figure 5B, Figure S4,

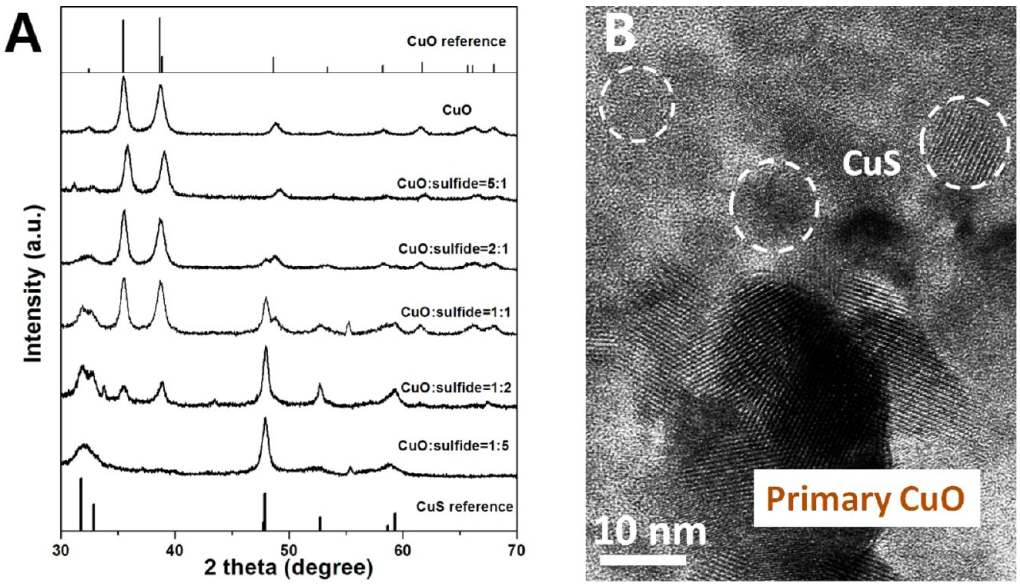

Figure 5. Phases and morphologies of the solid products from reaction of CuO-NPs with soluble HS^-. (A) XRD patterns of sulfidated CuO nanoparticles generated from initial Cu/S ratios that vary from 0.2 to 5. CuO (tenorite) and CuS (covellite) reference is presented for comparison. Please note the CuO/CuS peak intensity ratio cannot be used to calculate the percentage of CuS produced, but it can show a general trend that CuS produced increase with decreasing CuO to bisulfide ratio. (B) HRTEM image of sulfidated CuO nanoparticles (generated from 2.5 mM of CuO-NPs incubated in 5 mM Na_2S solution for one day), corresponding to a CuO/bisulfide molar ratio of 1:2. The images show the formation of small secondary particles with size 5–10 nm and showing lattice fringes indicating the presence of at least some crystalline products.

Supporting Information). The theoretical amount of bisulfide needed to stoichiometrically convert CuO to CuS is only at the ratio 1:1, but the data in Figure 5 only achieve complete sulfidation at the ratio 5:1, so either sulfidation is limited by kinetics, or there are competing reactions for bisulfide (*vida infra*).

We carried out additional experiments to understand the sulfidation mechanism and reaction stoichiometry. The presence of small particles surrounding a central core suggests a dissolution–precipitation mechanism rather than a direct solid-state exchange reaction. Recent research has reported dissolution–precipitation mechanism for the sulfidation of ZnO NPs[32] with similar morphologies in the sulfidation products.

To better understand sulfidation pathways, we interrupted the sulfidation process and examined the soluble products or clusters (after half hour incubation) that passed through a 200 nm syringe filter.[72] Figure 6B shows UV–vis spectra of this filtrate after aging for up to 3 h, which shows an absorption feature that starts to appear around 600 nm that likely belongs to CuS.[73] The aged filtrate was washed three times with water and then concentrated for DLS analysis (Figure 6C), which shows 10 nm mean particle size. These are much smaller than the starting CuO-NPs (50 nm), suggesting they are secondary particles/clusters formed by dissolution–precipitation. XRD analysis identifies them as CuS (Figure 6D). We also investigated the filtrate of the solution after 3 h incubation and did not observe the characteristic CuS peak, which suggests these ultrafine CuS clusters have grown or else attached to larger particles.[40] As a control we incubated CuO-NPs in NaOH at the same pH (9.3) as the sulfide solutions (but without sulfide) and performed the ultrafiltration, but we did not see particles/clusters in the filtrate. The filtrate from this control was treated with sulfide, and the product was investigated with UV–vis, but no characteristic CuS peak was observed. In another separate experiment, the filtrate was digested with nitric acid and prepared for ICP-AES analysis to determine the copper concentration. No detectable copper was found in the filtrate by ICP-AES. Together these data indicate that CuO-NPs undergo rapid sulfidation and the mechanism involves dissolution–precipitation. However, the detection of secondary CuS nanoparticles does not exclude the possibility of some direct solid-phase conversion. It is interesting that this can even occur at high pH (9.3) where CuO dissolution is extremely limited. Bisulfide is a high-affinity ligand for ionic copper, and the data indicate that it promotes copper dissolution from CuO-NPs at the same time it forms the insoluble CuS phases as secondary particles in the immediate vicinity of the mobilization sites. The dual role of bisulfide as dissolution promoter and precipitating agent explain the essential behavior in Figure 6.

Properties of CuS—Catalysis of Sulfide Oxidation. The data in Figure 5 show that a great excess of bisulfide is needed to fully convert CuO-NPs to CuS. While this could indicate kinetic limitations for this reaction, we instead have evidence that it is due to bisulfide consumption by oxygen that is catalyzed by the same CuS that is produced as the sulfidation product. In time-resolved

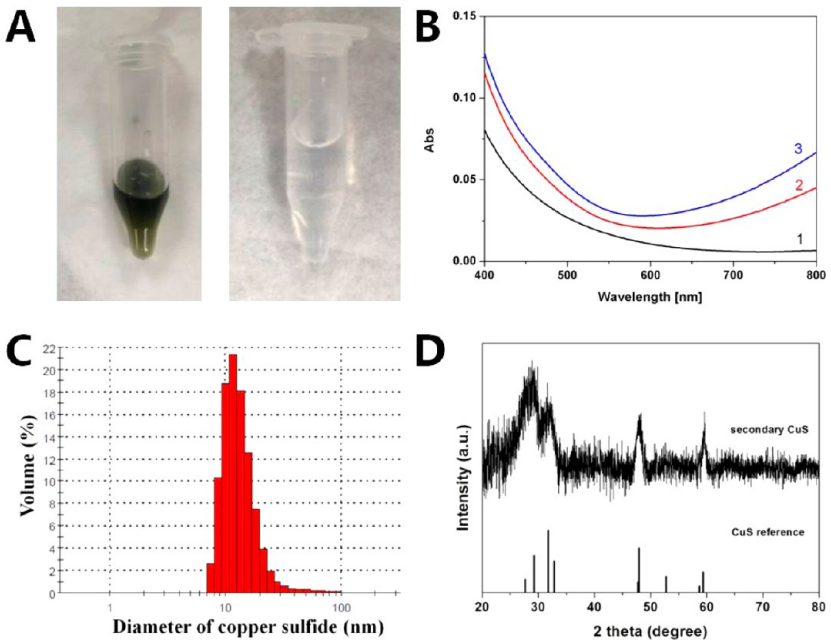

Figure 6. (A) Optical images of concentrated secondary CuS particles through 200 nm filter (left) and the filtrate after CuO-NPs suspension in NaOH solution through 200 nm filter (right). (B) UV−vis spectra shows formation of CuS nanoparticles. Curves 1, 2, 3 correspond to aging for 0, 1, 3 h, respectively. (C) The size distribution of secondary CuS determined by DLS. The original mean size of CuO nanoparticles is 50 nm. (D) XRD pattern confirms the formation of CuS. In these experiments, Na_2S and CuO-NPs were incubated at a molar ratio of 2:1.

studies we observed a rapid depletion of bisulfide upon addition of copper oxide nanoparticles (Figure S5A, Supporting Information), even if the bisulfide concentration was 5 times greater than the Cu on a molar basis. This cannot be explained by CuS precipitation stoichiometry, and instead must indicate either superstoichiometric sulfide phases or catalytic loss of bisulfide by oxidation. The XRD results show CuS as a main product, so bisulfide oxidation seemed more likely. To test this hypothesis, we added copper chloride (the concentration is 0.1, 1, or 2 mM, respectively) to existing excess bisulfide solutions and saw rapid drops in dissolved oxygen concentration (Figure 7A). The O_2 depletion rate increased with increasing Cu^{2+} addition. Copper ion has been shown to catalyze the oxidation of bisulfide in the presence of oxygen,[74] and the reduction of Cu(II) to Cu(I) has been observed on the surface of CuO when incubated in bisulfide solutions.[75] However, in our experiments it was still not clear whether dissolved copper ions or CuO nanoparticles were the active catalyst. To investigate this, the catalytic ability of CuO nanoparticles was compared with that of equimolar Cu ion in excess bisulfide solution, and the depletion of bisulfide was also monitored at the same time. Figure S5B (Supporting Information) shows the depletion of bisulfide is much faster in the presence of free Cu ion than the presence of CuO nanoparticles. Therefore, catalytic ability of CuO nanoparticles in bisulfide oxidation is not significant. Further, the oxygen concentrations were unchanged if copper ion was added in equimolar amounts to HS^- to make stoichiometric CuS, which indicated copper ions readily reacted with bisulfide before catalyzing the oxidation of bisulfide. Overall it is clear that CuS is the catalytic phase for bisulfide oxidation.[76] Comparison experiments indicated both the soluble CuS clusters and CuS particles contribute to the catalytic oxidation of bisulfide in the presence of oxygen (Figure S5C, Supporting Information).

Implications for Cu-NP Toxicity. The environmental transformation of a nanomaterial immediately raises questions about the behavior and toxicity of the transformed product(s), which may represent a greater or less risk than the original material. Metal sulfidation is often regarded as a passivation or detoxification process[57,58] due to the very low equilibrium solubilities and thus metal bioavailabilities of the sulfide phases (Figure 1).

We were also surprised, however, to observe that CuS-NPs and sulfidated CuO-NPs continued to show redox activity in our EPR Fenton assay (Figure S5C, Supporting Information, Figure 7C). These CuS-NPs were made by Cu^{2+}/S^{2-} precipitation processes, and the excess ions were removed by water washing prior to the ROS assay. Here again soluble species were the source of the redox activity, as evidenced by comparing the particle-induced ROS to that of filtrate, which were similar (Figure 7C). Although CuS is highly insoluble, the ROS assay uses H_2O_2 as a reactant, and we hypothesized that the soluble, redox-active species were copper ions produced by peroxide oxidation of CuS. Sulfide can be oxidized, and the conversion to

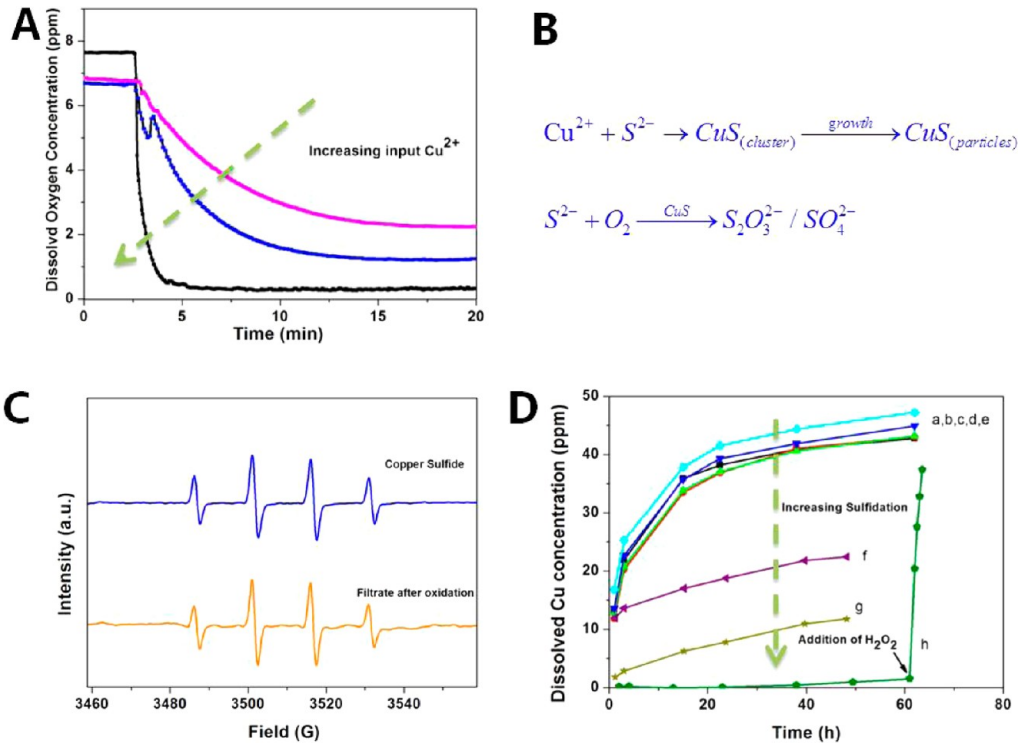

Figure 7. Properties of sulfidated CuO-NPs and implications for toxicity. (A,B) CuS clusters and nanoparticles serve as catalysts for bisulfide oxidation. Reaction tracked through depletion of dissolved oxygen upon addition of copper ions to excess Na_2S solution. Pink, blue, and black curves correspond to addition of 0.1, 1, or 2 mM copper ion. (C) Hydroxyl radical EPR signal induced by a 0.1 mM CuS suspension and its particle-free filtrate after hydrogen peroxide treatment. Despite low solubility, CuS shows redox activity associated with soluble species. (D) Dissolution behavior of CuS and a series of partially sulfidated CuO-NPs at pH 4 acetate buffer. The sulfidation was carried out using 2.5 mM CuO at the initial S/Cu ratios from 0.2 to 5. (a, b, c, d, e represent the dissolution of CuO, sulfidated CuO with S/Cu at 0.1, 0.2, 0.5, and 1, which has little effect on CuO dissolution; f, g represent the dissolution behavior of sulfidated CuO with S/Cu at 2, 5, respectively, which can slow the dissolution rate.) The pure CuS solid (represented by h) was prepared through precipitation of Cu^{2+} and bisulfide in stoichiometric mixture followed by washing and resuspension. To understand the redox behavior in (C), the oxidative-dissolution of CuS was investigated by adding H_2O_2 solution in equimolar proportion to CuS.

oxidized sulfur species may destabilize copper in the CuS lattice and lead to ion release and solution-based Fenton activity.

To pursue this hypothesis, we studied copper mobilization from CuS-NPs and a series of partially sulfidated CuO-NPs (Figure 7D). Partial sulfidation has almost no effect on the rate of copper release from the CuO-NPs undergoing transformation (bisulfide:CuO ratios from 1:5 up to 1:1). It is clear that partial sulfidation does not passivate CuO surfaces, which is consistent with the dissolution−precipitation mechanism that produces distinct secondary particles rather than protective coatings. Only at bisulfide:CuO ratios above 2:1 do we begin to see reductions in soluble copper release. The model CuS nanoparticles formed from Cu^{2+} and S^{2-} showed very low copper ion release, as expected, but addition of H_2O_2 at the 60 h time point caused significant release (Figure 7D, green circles). In fact, EPR results suggest much more copper ions released from CuS than CuO when both were exposed to H_2O_2 at the same pH. These data provide support for CuS oxidation by H_2O_2 as the source of the redox activity seen in the EPR spectra of Figure 7C. The combined results suggest that sulfidation of Cu-NPs or CuO-NPs can reduce copper metal bioavailability, but only if the sulfidation is extensive and progresses to near stoichiometric completion, and oxidation with rerelease of soluble copper may prevent CuS from being a fully nontoxic end state for copper-containing nanomaterials in the environment. Others have reported that nanoscale Cu and Zn sulfides are not fully stable and can transform into other species under aerobic conditions.[77,78]

Finally, we were interested in the biological implications of copper material transformations, and the effects of sulfidation on toxicity in particular. Previous studies showed that copper nanoparticles are internalized by target cells and release soluble ions more rapidly than micrometer-sized particles at the acidic pH in lysosomes as predicted by the "Trojan-horse mechanism" for metallic nanoparticle toxicity.[33,79] Here, uptake and toxicity of CuO- and CuS-NPs were assessed using a murine macrophage cell line in cell culture in comparison with carbon black nanoparticles as a nontoxic particle control. Following exposure to test and control particles for 3 h, well-dispersed particles were visualized in the cytoplasm of target cells (Figure 8A). Cell viability was assessed after 24 h using a combination of brightfield (Figure 8B) and fluorescence

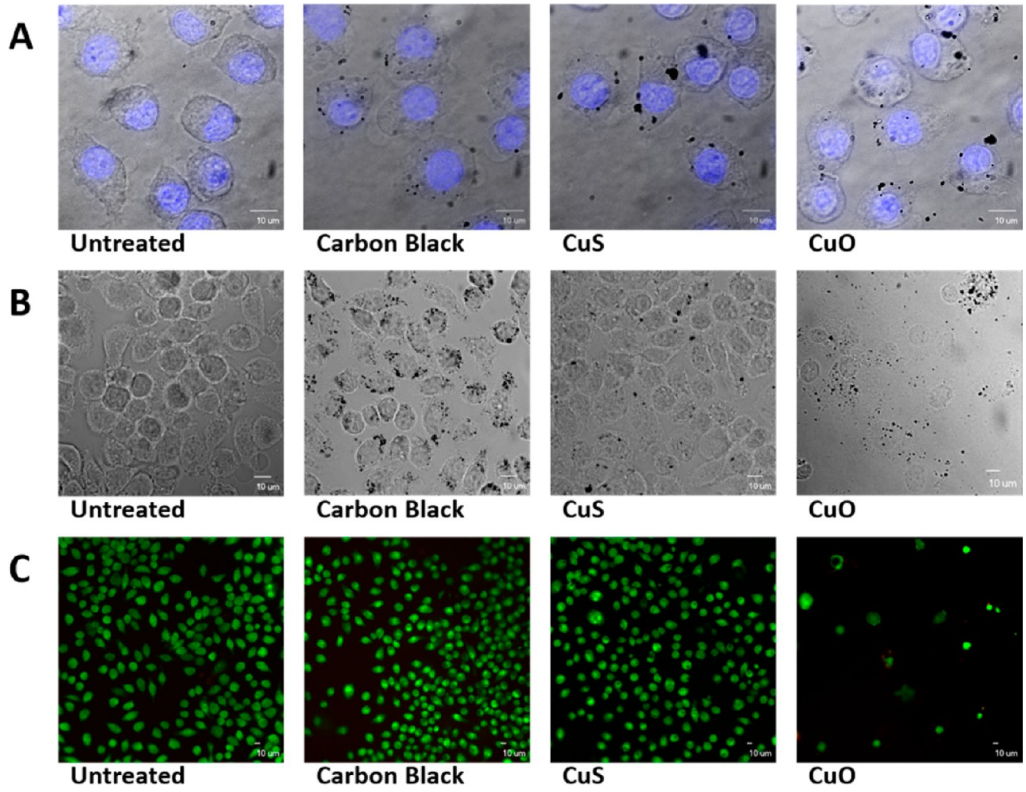

Figure 8. Target cell uptake and toxicity of carbon black, CuS, and CuO-NPs. (A) Confocal images of murine macrophages after exposure to 5 ppm of test particles for 3 h; nuclei were visualized (blue fluorescence) using 4′6-diamidino-2-phenylindole (DAPI). (B) Brightfield microscopic images of murine macrophages 24 h after exposure to 5 ppm of test nanoparticles. (C) Viability of target cells 24 h after exposure to 5 ppm of test nanoparticles. Viable cells show green cytoplasmic fluorescence (Syto 10/ethidium homodimer assay).

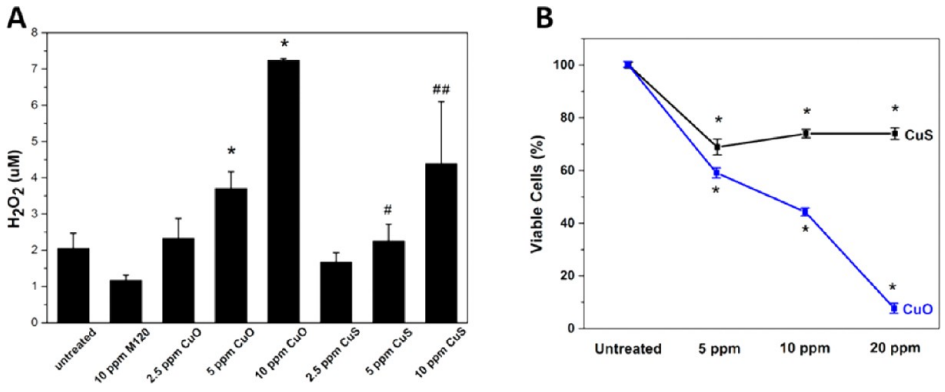

Figure 9. (A) Generation of H_2O_2 by murine macrophages exposed to carbon black, CuO- and CuS-NPs. Detection of H_2O_2 production in macrophages exposed to 2.5, 5, or 10 ppm of CuO, CuS, or M120 (carbon black) as determined using the Amplex Red assay 20 min after exposure. Cells exposed to higher concentrations of CuO demonstrate significantly increased generation of H_2O_2 compared to untreated controls or CuS-exposed cells. *$p < 0.05$ compared to control; $^{\#}p < 0.05$ compared to 5 ppm CuO; $^{\#\#}p < 0.05$ compared to 10 ppm CuO. (B) Viability of murine macrophages after exposure to CuS-NPs or CuO-NPs for 48 h. DNA content relative to untreated control cells was determined using Pico Green fluorescence as a surrogate for cell number. Differences in viability of cells exposed to each dose of CuS- or CuO-NPs relative to untreated controls was statistically significant after 48 h. *$p < 0.05$ compared to control.

(Figure 8C) microscopy. Only CuO-NPs induced cell death and detachment after 24 h. Intracellular mobilization of Cu ions induces redox cycling resulting in generation of ROS, induction of oxidative stress, and cell death.[80] Delivery of CuO- or CuS-NPs triggered generation of higher levels of H_2O_2 in murine macrophages after 20 min compared to untreated cells or cells exposed to carbon black NPs (Figure 9A). Over the same range of doses, CuO-NPs induced significantly higher toxicity than CuS-NPs after 24 h (Figure S7, Supporting Information) and 48 h (Figure 9B), consistent with the lower Cu bioavailability in CuS.

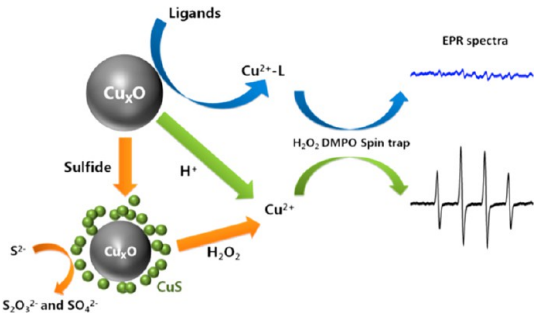

Figure 10. Summary of chemical transformations and redox behaviors of Cu-based nanoparticles in biological and environmental media.

CONCLUSIONS

Copper-containing nanomaterials are a particularly complex case for EHS studies, since they undergo oxidation, dissolution, sulfidation, and further oxidation of the sulfide phases over the time scales relevant for human health and environmental impacts. Figure 10 summarizes the main transformation and redox pathways observed for CuO-NPs in this study. CuO-NPs or oxide films on metallic Cu-NPs dissolve at low pH, or at neutral pH in the presence of ligands in biological environments, including those containing amine functional groups. The redox activity in copper NP systems appears to be associated with the soluble fraction and is mitigated but not eliminated by ligand binding in solution. CuO-NPs undergo sulfidation through a dissolution/precipitation mechanism to produce complex secondary aggregates of CuS-NPs. These CuS-NPs are active catalysts for bisulfide oxidation. Sulfidation reduces Cu solubility, redox activity, and cytotoxicity but may not necessarily fully and permanently detoxify copper, since CuS can be oxidized in environments containing H_2O_2 to produce free copper that continues to cycle in solution producing hydroxyl radicals through Fenton-like chemistry. The results are directly relevant for CuO-NPs and may also be qualitatively relevant for elemental nanocopper whose surfaces consist of oxide phases following environmental exposure.

MATERIALS AND METHODS

CuO-NP agents were purchased from Aldrich and used as received. The CuO nanoparticles were synthesized using the molten salt synthesis method according to the manufacturer, and some organic matter was observed on the surface according to FT-IR (Figure S1B, Supporting Information). Phosphate buffered saline (PBS buffer, 10×) was obtained from Fisher Scientific (MA, USA) and diluted with deionized (DI) water before use. The particles were characterized for size (mean 50 nm determined by TEM), surface charge in PBS buffer (zeta potential −25 mV), size distribution in PBS buffer and crystalline phase (tenorite) (Figure S1, Supporting Information). The increased size of particles in PBS buffer indicated the aggregation of CuO nanoparticles.

CuO Dissolution Experiments. CuO-NPs (200 ppm) were incubated in biologically or environmentally relevant media that included acetate buffers (50 mM, pH 4, 5, and 6), PBS buffer (1× concentration, pH 7.4), and borate buffers (50 mM, pH 8 and 9) for pH control. Acetate buffer (pH 4.9) was used as lysosome-mimic, and DMEM and RPMI cell culture media were studied supplemented with 10% FBS. The use of simulant fluids in environmental and biological studies has many limitations, but does provide well-defined environments for studying the chemical transformations of materials.[81] Nanoparticles were dispersed by 15 min sonication in 5 mL of the solutions. After incubating for a predefined time period, the samples were centrifuged by centrifugal ultrafiltration (Amicon Ultra-4 3k) for 30 min at 4000 rpm to remove the solids, and the supernatant was separated for determination of Cu concentration by ICP-AES. All ion release experiments were conducted at room temperature (20 °C) unless noted. The ability of centrifugal ultrafiltration to remove the nanoparticles has been proved by previous reference.[49] Our control experiments show ultrafiltration can effectively remove CuO nanoparticles, and the Cu ions retention by the ultrafiltration filters can be neglected (Figure S6, Supporting Information). Therefore, solubility is defined as free metal ions and its complex, which is almost the same as all forms of metal that pass through the ultrafiltration filters in our case.

Electron Paramagnetic Resonance ROS Assay. The ability of CuO-NPs and/or associated soluble species to generate hydroxyl radical in the presence of H_2O_2 were quantified using X (9.8 GHz)-band EPR measurements at room temperature using an EMX-plus CW spectrometer (Bruker Biospin) and the spin-trap DMPO (Dojindo Molecular Technologies, Inc.). In a typical experiment, 2 or 20 ppm CuO-NPs were incubated with 100 mM DMPO, 1 mM H_2O_2 in PBS buffer (pH 7.4) for 20 min, and the reaction was initiated by addition of H_2O_2. Then the aqueous solution was drawn into 50 μL capillary (Cat No. 53432-783, VWR), and the capillary was inserted into a quartz EPR capillary tube (4 mm OD × 250 mm L × 0.5 mm wall, Wilmad LabGlass, Buena, NJ). The data acquisition parameters were set as follows: Center Field, 3508.75 G; sweep width, 100 G; sweep time, 30 s; modulation amplitude, 1 G; number of scans, 10; microwave power, 2 mW; conversion time, 30 ms; time constant, 81.92 ms. Though EPR cannot quantitatively measure the radical produced because of decomposition of DMPO−OH adduct, it can give a relative ROS intensity by comparing the peak height if the incubation time and instrument parameters are constant.

Sulfide and Dissolved Oxygen (DO) Depletion Measurements. The sulfidation of CuO-NPs were studied by tracking sulfide depletion using the method of Liu *et al.*[41] Soluble sulfide concentration was measured with a sulfide-ion-selective electrode following removal of solids by centrifugal ultrafiltration (Amicon Ultra-4 3k). In a typical experiment, 1 mg of CuO-NP powder was added to 4.5 mL of DI water, followed with sonication for 15 min to disperse the aggregates, and then 0.5 mL of 125 mM Na_2S solution was added to initiate the reaction at a starting sulfide concentration of 12.5 mM. The pH of 12.5 mM Na_2S solution is around 9.3, where the main soluble sulfide species is bisulfide (HS^-). After rotating the mixture for a predetermined time, the bisulfide solution was separated by centrifugal ultrafiltration, and the sulfide antioxidant buffer (ASOB, Orion 941609 Thermo Scientific) was added to prevent bisulfide oxidation and volatilization before analysis. Bisulfide concentration in the filtrate was measured with sulfide-ISE (Orion 9616BNWP Silver/Sulfide combination electrode, Thermo Scientific) at room temperature. DO levels were monitored *in situ* during incubation of either copper ions or CuO-NPs in bisulfide solutions in a closed amber glass bottle under magnetic stirring using a DO probe (Orion 083010MD, Thermo Scientific) at 3 s sampling frequency.

Cell Toxicity Studies. An immortalized murine macrophage cell line, J774.A1 (ATCC number TIB-67) was used as a target cell for assessment of uptake, H_2O_2 generation, and toxicity of CuO- and CuS-NPs. Carbon black (M120, Cabot) with a primary particle diameter ~75 nm was used as a nontoxic reference particle. Test particles were dispersed in RPMI 1640 medium

containing 1% FBS at a concentration of 250 ppm and sonicated at 100 W in a Branson 2510 sonicating water bath for 60 min prior to dilution at final concentrations of 5−20 ppm in cell culture medium. Murine macrophages were cultured in RPMI 1640 medium (Invitrogen 11875) containing 10% FBS, 2 mM glutamine, 1 mM sodium pyruvate, and 500 μL of penicillin−streptomycin in ultralow attachment culture dishes (Corning 3262) at 37 °C in air with 5% CO_2. For microscopy, cells were plated on glass coverslips in 12 well plates (Coster, 22 mm in diameter) at 70% confluence, allowed to attach for 3 h, and then exposed to test particles for 3−24 h. To visualize uptake of test particles, cells were rinsed and stained with 4′6-diamidino-2-phenylindole (DAPI) and visualized under brightfield and fluorescence illumination using a spinning disk Olympus confocal inverted microscope (Model 1X81). To assess viability, cells were visualized using brightfield imaging to assess morphology and cell detachment and confirmed by staining with 1:1000 Syto 10/ethidium homodimer (Invitrogen) for 5 min. Viable (green fluorescence) and dead cells (red fluorescence) were imaged using a spinning disk Olympus confocal inverted microscope equipped with fluorescence filters. Cell viability using DNA content as a surrogate for cell number was quantitated using a fluorescence assay (Pico Green, Invitrogen) that quantitatively binds to DNA according to the manufacturer's instructions. For quantitation of H_2O_2 generation, murine macrophages were seeded in RPMI growth medium at 75 000 cells per well in a black clear bottom 96-well plate (Costar 3603). Cells were allowed to equilibrate overnight at 37 °C, after which growth medium was aspirated and subsequently replaced with 200 μL of medium per well containing 50 μM Amplex Red reagent (Invitrogen A1222), 2 μL of 10 U/mL horse radish peroxidase (Invitrogen 012001), and 2.5, 5, and 10 ppm of test particles.[82] Continuous fluorescence measurements were obtained using a spectrophotometer with an excitation of 566 nm and an emission of 587 nm. Data were acquired every 5 min and reported after 20 min of exposure to test particles. Statistical significance was determined using an unpaired *t*-test to compare differences between the means (±SD) of untreated and treated cultures in triplicate. A *p*-value of <0.05 was considered to be statistically significant.

Product Characterization. UV−vis spectra of sulfidated CuO-NP samples were recorded on a V-630 spectrophotometer (Jasco, MD) over the range 400 to 800 nm. The sizes of secondary CuS particles (formed by dissolution and precipitation) were monitored using dynamic light scattering (DLS) with a Zetasizer Nano ZS system (Malvern Instruments). The morphologies of the sulfidated CuO-NPs were observed in high-resolution transmission electron microscopy (HRTEM) on a JEOL JEM-2010. The samples were prepared by placing one drop of purified sample solution on carbon-coated copper grids, followed by drying at room temperature overnight. The compositions and phases of sulfidated CuO samples were identified by X-ray diffraction spectrometry (XRD) on a Bruker AXS D8 Advance instrument with Cu Kα radiation (λ = 1.5418 Å). The XRD samples were prepared by adding purified and concentrated sulfidated CuO nanoparticles suspension onto a glass slide, followed by overnight drying.

Conflict of Interest: The authors declare no competing financial interest.

Acknowledgment. This work was supported by the National Science Foundation (Grant ECCS-1057547), the Superfund Research Program of the National Institute of Environmental Health Sciences (P42 ES013660), and a Training Grant from the National Institute of Environmental Health Sciences (T32 ES007272). The authors acknowledge discussions and technical assistance from Dr. Jingyu Liu, Joseph Orchardo, and Anthony McCormick.

Supporting Information Available: Additional details about Visual MINTEQ 3.0 calculations, characterization of commercial CuO nanoparticles, time-dependent dissolution of CuO nanoparticles in PBS buffer (pH 7.4), the effects of various components in cell culture media on the dissolution of CuO in PBS buffer, hydroxyl radical induced by 0.032 ppm Cu^{2+} with 1 mM glutamine in PBS buffer after 20, 45, and 95 min incubation, HRTEM image of sulfidated CuO nanoparticles showing the lattice fringes, sulfidation of CuO-NPs and the catalytic ability of CuS, and viability of murine macrophages exposed to 5, 10, or 20 ppm of carbon black, CuO-, and CuS-NPs for 24 h. This material is available free of charge *via* the Internet at http://pubs.acs.org.

REFERENCES AND NOTES

1. Evans, P.; Matsunaga, H.; Kiguchi, M. Large-Scale Application of Nanotechnology for Wood Protection. *Nat. Nanotechnol.* **2008**, *3*, 577–577.
2. Wu, Y.; Wadia, C.; Ma, W.; Sadtler, B.; Alivisatos, A. P. Synthesis and Photovoltaic Application of Copper(I) Sulfide Nanocrystals. *Nano Lett.* **2008**, *8*, 2551–2555.
3. Youngil, L.; Jun-rak, C.; Kwi Jong, L.; Nathan, E. S.; Donghoon, K. Large-Scale Synthesis of Copper Nanoparticles by Chemically Controlled Reduction for Applications of Inkjet-Printed Electronics. *Nanotechnology* **2008**, *19*, 415604.
4. Ren, G.; Hu, D.; Cheng, E. W. C.; Vargas-Reus, M. A.; Reip, P.; Allaker, R. P. Characterisation of Copper Oxide Nanoparticles for Antimicrobial Applications. *Int. J. Antimicrob. Agents* **2009**, *33*, 587–590.
5. PandeyA; BrovelliS; ViswanathaR; LiL; Pietryga, J. M.; Klimov, V. I.; Crooker, S. A. Long-Lived Photoinduced Magnetization in Copper-Doped Znse-Cdse Core-Shell Nanocrystals. *Nat. Nanotechnol.* **2012**, 792–797.
6. Maithreepala, R. A.; Doong, R.-a. Reductive Dechlorination of Carbon Tetrachloride in Aqueous Solutions Containing Ferrous and Copper Ions. *Environ. Sci. Technol.* **2004**, *38*, 6676–6684.
7. Doong, R.-a.; Chang, S.-m.; Tsai, C. W. Enhanced Photoactivity of Cu-Deposited Titanate Nanotubes for Removal of Bisphenol A. *Appl. Catal., B* **2013**, *129*, 48–55.
8. Huang, H.-L.; Wang, H. P.; Wei, G.-T.; Sun, I. W.; Huang, J.-F.; Yang, Y. W. Extraction of Nanosize Copper Pollutants with an Ionic Liquid. *Environ. Sci. Technol.* **2006**, *40*, 4761–4764.
9. Zhang, H.; Ji, Z.; Xia, T.; Meng, H.; Low-Kam, C.; Liu, R.; Pokhrel, S.; Lin, S.; Wang, X.; Liao, Y.-P.; *et al.* Use of Metal Oxide Nanoparticle Band Gap to Develop a Predictive Paradigm for Oxidative Stress and Acute Pulmonary Inflammation. *ACS Nano* **2012**, *6*, 4349–4368.
10. Mudunkotuwa, I. A.; Pettibone, J. M.; Grassian, V. H. Environmental Implications of Nanoparticle Aging in the Processing and Fate of Copper-Based Nanomaterials. *Environ. Sci. Technol.* **2012**, *46*, 7001–7010.
11. Li, Y.; Zhang, W.; Niu, J.; Chen, Y. Mechanism of Photogenerated Reactive Oxygen Species and Correlation with the Antibacterial Properties of Engineered Metal-Oxide Nanoparticles. *ACS Nano* **2012**, *6*, 5164–5173.
12. Applerot, G.; Lellouche, J.; Lipovsky, A.; Nitzan, Y.; Lubart, R.; Gedanken, A.; Banin, E. Understanding the Antibacterial Mechanism of CuO Nanoparticles: Revealing the Route of Induced Oxidative Stress. *Small* **2012**, *8*, 3326–3337.
13. Gunawan, C.; Teoh, W. Y.; Marquis, C. P.; Amal, R. Cytotoxic Origin of Copper(II) Oxide Nanoparticles: Comparative Studies with Micron-Sized Particles, Leachate, and Metal Salts. *ACS Nano* **2011**, *5*, 7214–7225.
14. Studer, A. M.; Limbach, L. K.; Van Duc, L.; Krumeich, F.; Athanassiou, E. K.; Gerber, L. C.; Moch, H.; Stark, W. J. Nanoparticle Cytotoxicity Depends on Intracellular Solubility: Comparison of Stabilized Copper Metal and Degradable Copper Oxide Nanoparticles. *Toxicol. Lett.* **2010**, *197*, 169–174.
15. Karlsson, H. L.; Cronholm, P.; Gustafsson, J.; Moller, L. Copper Oxide Nanoparticles Are Highly Toxic: A Comparison between Metal Oxide Nanoparticles and Carbon Nanotubes. *Chem. Res. Toxicol.* **2008**, *21*, 1726–1732.
16. Ahamed, M.; Siddiqui, M. A.; Akhtar, M. J.; Ahmad, I.; Pant, A. B.; Alhadlaq, H. A. Genotoxic Potential of Copper Oxide Nanoparticles in Human Lung Epithelial Cells. *Biochem. Biophys. Res. Commun.* **2010**, *396*, 578–583.
17. Fahmy, B.; Cormier, S. A. Copper Oxide Nanoparticles Induce Oxidative Stress and Cytotoxicity in Airway Epithelial Cells. *Toxicol. In Vitro* **2009**, *23*, 1365–1371.

18. Jo, H. J.; Choi, J. W.; Lee, S. H.; Hong, S. W. Acute Toxicity of Ag and CuO Nanoparticle Suspensions against Daphnia Magna: The Importance of their Dissolved Fraction Varying with Preparation Methods. *J. Hazard. Mater.* **2012**, *227−228*, 301–308.
19. Lowry, G. V.; Gregory, K. B.; Apte, S. C.; Lead, J. R. Transformations of Nanomaterials in the Environment. *Environ. Sci. Technol.* **2012**, *46*, 6893–6899.
20. Borm, P.; Klaessig, F. C.; Landry, T. D.; Moudgil, B.; Pauluhn, J.; Thomas, K.; Trottier, R.; Wood, S. Research Strategies for Safety Evaluation of Nanomaterials, Part V: Role of Dissolution in Biological Fate and Effects of Nanoscale Particles. *Toxicol. Sci.* **2006**, *90*, 23–32.
21. Reidy, B.; Haase, A.; Luch, A.; Dawson, K.; Lynch, I. Mechanisms of Silver Nanoparticle Release, Transformation and Toxicity: A Critical Review of Current Knowledge and Recommendations for Future Studies and Applications. *Materials* **2013**, *6*, 2295–2350.
22. Liu, J.; Wang, Z.; Liu, F. D.; Kane, A. B.; Hurt, R. H. Chemical Transformations of Nanosilver in Biological Environments. *ACS Nano* **2012**, *6*, 9887–9899.
23. Levard, C.; Hotze, E. M.; Lowry, G. V.; Brown, G. E. Environmental Transformations of Silver Nanoparticles: Impact on Stability and Toxicity. *Environ. Sci. Technol.* **2012**, *46*, 6900–6914.
24. Lowry, G. V.; Espinasse, B. P.; Badireddy, A. R.; Richardson, C. J.; Reinsch, B. C.; Bryant, L. D.; Bone, A. J.; Deonarine, A.; Chae, S.; Therezien, M.; *et al.* Long-Term Transformation and Fate of Manufactured Ag Nanoparticles in a Simulated Large Scale Freshwater Emergent Wetland. *Environ. Sci. Technol.* **2012**, *46*, 7027–7036.
25. Kent, R. D.; Vikesland, P. J. Controlled Evaluation of Silver Nanoparticle Dissolution Using Atomic Force Microscopy. *Environ. Sci. Technol.* **2011**, *46*, 6977–6984.
26. Kennedy, A. J.; Hull, M. S.; Bednar, A. J.; Goss, J. D.; Gunter, J. C.; Bouldin, J. L.; Vikesland, P. J.; Steevens, J. A. Fractionating Nanosilver: Importance for Determining Toxicity to Aquatic Test Organisms. *Environ. Sci. Technol.* **2010**, *44*, 9571–9577.
27. Stebounova, L.; Guio, E.; Grassian, V. Silver Nanoparticles in Simulated Biological Media: A Study of Aggregation, Sedimentation, and Dissolution. *J. Nanopart. Res.* **2011**, *13*, 233–244.
28. Sotiriou, G. A.; Pratsinis, S. E. Antibacterial Activity of Nanosilver Ions and Particles. *Environ. Sci. Technol.* **2010**, *44*, 5649–5654.
29. Lorenz, C.; Windler, L.; von Goetz, N.; Lehmann, R. P.; Schuppler, M.; Hungerbühler, K.; Heuberger, M.; Nowack, B. Characterization of Silver Release from Commercially Available Functional (Nano)Textiles. *Chemosphere* **2012**, *89*, 817–824.
30. Xia, T.; Zhao, Y.; Sager, T.; George, S.; Pokhrel, S.; Li, N.; Schoenfeld, D.; Meng, H.; Lin, S.; Wang, X.; *et al.* Decreased Dissolution of ZnO by Iron Doping Yields Nanoparticles with Reduced Toxicity in the Rodent Lung and Zebrafish Embryos. *ACS Nano* **2011**, *5*, 1223–1235.
31. Franklin, N. M.; Rogers, N. J.; Apte, S. C.; Batley, G. E.; Gadd, G. E.; Casey, P. S. Comparative Toxicity of Nanoparticulate ZnO, Bulk ZnO, and $ZnCl_2$ to a Freshwater Microalga (*Pseudokirchneriella subcapitata*): The Importance of Particle Solubility. *Environ. Sci. Technol.* **2007**, *41*, 8484–8490.
32. Ma, R.; Levard, C.; Michel, F. M.; Brown, G. E.; Lowry, G. V. Sulfidation Mechanism for Zinc Oxide Nanoparticles and the Effect of Sulfidation on their Solubility. *Environ. Sci. Technol.* **2013**, *47*, 2527–2534.
33. Midander, K.; Cronholm, P.; Karlsson, H. L.; Elihn, K.; Möller, L.; Leygraf, C.; Wallinder, I. O. Surface Characteristics, Copper Release, and Toxicity of Nano- and Micrometer-Sized Copper and Copper(II) Oxide Particles: A Cross-Disciplinary Study. *Small* **2009**, *5*, 389–399.
34. Pettibone, J. M.; Adamcakova-Dodd, A.; Thorne, P. S.; O'Shaughnessy, P. T.; Weydert, J. A.; Grassian, V. H. Inflammatory Response of Mice Following Inhalation Exposure to Iron and Copper Nanoparticles. *Nanotoxicology* **2008**, *2*, 189–204.
35. Sotiriou, G. A.; Meyer, A.; Knijnenburg, J. T. N.; Panke, S.; Pratsinis, S. E. Quantifying the Origin of Released Ag+ Ions from Nanosilver. *Langmuir* **2012**, *28*, 15929–15936.
36. Yamamoto, K.; Kawanishi, S. Hydroxyl Free Radical Is Not the Main Active Species in Site-Specific DNA Damage Induced by Copper (II) Ion and Hydrogen Peroxide. *J. Biol. Chem.* **1989**, *264*, 15435–15440.
37. Drouin, R.; Rodriguez, H.; Gao, S.-W.; Gebreyes, Z.; O'Connor, T. R.; Holmquist, G. P.; Akman, S. A. Cupric Ion/Ascorbate/Hydrogen Peroxide-Induced DNA Damage: DNA-Bound Copper Ion Primarily Induces Base Modifications. *Free Radical Biol. Med.* **1996**, *21*, 261–273.
38. Erickson, R. J.; Benoit, D. A.; Mattson, V. R.; Leonard, E. N.; Nelson, H. P. The Effects of Water Chemistry on the Toxicity of Copper to Fathead Minnows. *Environ. Toxicol. Chem.* **1996**, *15*, 181–193.
39. Cabot, A.; Smith, R. K.; Yin, Y.; Zheng, H.; Reinhard, B. r. M.; Liu, H.; Alivisatos, A. P. Sulfidation of Cadmium at the Nanoscale. *ACS Nano* **2008**, *2*, 1452–1458.
40. Levard, C.; Reinsch, B. C.; Michel, F. M.; Oumahi, C.; Lowry, G. V.; Brown, G. E. Sulfidation Processes of PVP-Coated Silver Nanoparticles in Aqueous Solution: Impact on Dissolution Rate. *Environ. Sci. Technol.* **2011**, *45*, 5260–5266.
41. Liu, J.; Pennell, K. G.; Hurt, R. H. Kinetics and Mechanisms of Nanosilver Oxysulfidation. *Environ. Sci. Technol.* **2011**, *45*, 7345–7353.
42. Kim, B.; Park, C.-S.; Murayama, M.; Hochella, M. F. Discovery and Characterization of Silver Sulfide Nanoparticles in Final Sewage Sludge Products. *Environ. Sci. Technol.* **2010**, *44*, 7509–7514.
43. Wiesner, M. R.; Lowry, G. V.; Casman, E.; Bertsch, P. M.; Matson, C. W.; Di Giulio, R. T.; Liu, J.; Hochella, M. F. Meditations on the Ubiquity and Mutability of Nano-Sized Materials in the Environment. *ACS Nano* **2011**, *5*, 8466–8470.
44. Zhu, H.; Wang, J.; Wu, D. Fast Synthesis, Formation Mechanism, and Control of Shell Thickness of CuS Hollow Spheres. *Inorg. Chem.* **2009**, *48*, 7099–7104.
45. Jiao, S.; Xu, L.; Jiang, K.; Xu, D. Well-Defined Non-Spherical Copper Sulfide Mesocages with Single-Crystalline Shells by Shape-Controlled Cu_2O Crystal Templating. *Adv. Mater.* **2006**, *18*, 1174–1177.
46. Liu, J.; Sonshine, D. A.; Shervani, S.; Hurt, R. H. Controlled Release of Biologically Active Silver from Nanosilver Surfaces. *ACS Nano* **2010**, *4*, 6903–6913.
47. Reinsch, B. C.; Levard, C.; Li, Z.; Ma, R.; Wise, A.; Gregory, K. B.; Brown, G. E.; Lowry, G. V. Sulfidation of Silver Nanoparticles Decreases *Escherichia coli* Growth Inhibition. *Environ. Sci. Technol.* **2012**, *46*, 6992–7000.
48. MacCuspie, R. Colloidal Stability of Silver Nanoparticles in Biologically Relevant Conditions. *J. Nanopart. Res.* **2011**, *13*, 2893–2908.
49. Liu, J.; Hurt, R. H. Ion Release Kinetics and Particle Persistence in Aqueous Nano-Silver Colloids. *Environ. Sci. Technol.* **2010**, *44*, 2169–2175.
50. Akaighe, N.; MacCuspie, R. I.; Navarro, D. A.; Aga, D. S.; Banerjee, S.; Sohn, M.; Sharma, V. K. Humic Acid-Induced Silver Nanoparticle Formation under Environmentally Relevant Conditions. *Environ. Sci. Technol.* **2011**, *45*, 3895–3901.
51. Pietruska, J. R.; Liu, X.; Smith, A.; McNeil, K.; Weston, P.; Zhitkovich, A.; Hurt, R.; Kane, A. B. Bioavailability, Intracellular Mobilization of Nickel, and Hif-1α Activation in Human Lung Epithelial Cells Exposed to Metallic Nickel and Nickel Oxide Nanoparticles. *Toxicol. Sci.* **2011**, *124*, 138–148.
52. Yang, X.; Gondikas, A. P.; Marinakos, S. M.; Auffan, M.; Liu, J.; Hsu-Kim, H.; Meyer, J. N. Mechanism of Silver Nanoparticle Toxicity is Dependent on Dissolved Silver and Surface Coating in *Caenorhabditis elegans*. *Environ. Sci. Technol.* **2011**, *46*, 1119–1127.
53. Li, X.; Lenhart, J. J.; Walker, H. W. Dissolution-Accompanied Aggregation Kinetics of Silver Nanoparticles. *Langmuir* **2010**, *26*, 16690–16698.
54. Ho, C.-M.; Yau, S. K.-W.; Lok, C.-N.; So, M.-H.; Che, C.-M. Oxidative Dissolution of Silver Nanoparticles by Biologically Relevant Oxidants: A Kinetic and Mechanistic Study. *Chem.—Asian J.* **2010**, *5*, 285–293.

55. Ho, C.-M.; Wong, C.-K.; Yau, S. K.-W.; Lok, C.-N.; Che, C.-M. Oxidative Dissolution of Silver Nanoparticles by Dioxygen: A Kinetic and Mechanistic Study. *Chem.—Asian J.* **2011**, *6*, 2506–2511.
56. Hirsch, M. P. Toxicity of Silver Sulfide-Spiked Sediments to the Freshwater Amphipod (*Hyalella azteca*). *Environ. Toxicol. Chem.* **1998**, *17*, 601–604.
57. Besser, J. M.; Ingersoll, C. G.; Giesty, J. P. Effects of Spatial and Temporal Variation of Acid-Volatile Sulfide on the Bioavailability of Copper and Zinc in Freshwater Sediments. *Environ. Toxicol. Chem.* **1996**, *15*, 286–293.
58. Di Toro, D. M.; Mahony, J. D.; Hansen, D. J.; Scott, K. J.; Hicks, M. B.; Mayr, S. M.; Redmond, M. S. Toxicity of Cadmium in Sediments: The Role of Acid Volatile Sulfide. *Environ. Toxicol. Chem.* **1990**, *9*, 1487–1502.
59. Bozym, R. A.; Chimienti, F.; Giblin, L. J.; Gross, G. W.; Korichneva, I.; Li, Y.; Libert, S.; Maret, W.; Parviz, M.; Frederickson, C. J.; Thompson, R. B. Free Zinc Ions outside a Narrow Concentration Range Are Toxic to a Variety of Cells *In Vitro*. *Exp. Biol. Med.* **2010**, *235*, 741–750.
60. Zhang, L.; Yu, J. C.; Yip, H. Y.; Li, Q.; Kwong, K. W.; Xu, A.-W.; Wong, P. K. Ambient Light Reduction Strategy to Synthesize Silver Nanoparticles and Silver-Coated TiO_2 with Enhanced Photocatalytic and Bactericidal Activities. *Langmuir* **2003**, *19*, 10372–10380.
61. Macomber, L.; Imlay, J. A. The Iron-Sulfur Clusters of Dehydratases are Primary Intracellular Targets of Copper Toxicity. *Proc. Natl. Acad. Sci. U. S. A.* **2009**, *106*, 8344–8349.
62. Chaturvedi, K. S.; Hung, C. S.; Crowley, J. R.; Stapleton, A. E.; Henderson, J. P. The Siderophore Yersiniabactin Binds Copper to Protect Pathogens During Infection. *Nat. Chem. Biol.* **2012**, *8*, 731–736.
63. Doğan, A.; Köseoğlu, F.; Klç, E. The Stability Constants of Copper(II) Complexes with Some α-Amino Acids in Dioxan−Water Mixtures. *Anal. Biochem.* **2001**, *295*, 237–239.
64. Deschamps, P.; Zerrouk, N.; Nicolis, I.; Martens, T.; Curis, E.; Charlot, M. F.; Girerd, J. J.; Prangé, T.; Bénazeth, S.; Chaumeil, J. C.; *et al.* Copper(II)−L-Glutamine Complexation Study in Solid State and in Aqueous Solution. *Inorg. Chim. Acta* **2003**, *353*, 22–34.
65. Szecsody, J. E.; Zachara, J. M.; Bruckhart, P. L. Adsorption-Dissolution Reactions Affecting the Distribution and Stability of Colledta in Iron Oxide-Coated Sand. *Environ. Sci. Technol.* **1994**, *28*, 1706–1716.
66. Joshi, S.; Ghosh, I.; Pokhrel, S.; Mädler, L.; Nau, W. M. Interactions of Amino Acids and Polypeptides with Metal Oxide Nanoparticles Probed by Fluorescent Indicator Adsorption and Displacement. *ACS Nano* **2012**, *6*, 5668–5679.
67. Oikawa, S.; Kawanishi, S. Site-Specific DNA Damage Induced by NADH in the Presence of Copper(II): Role of Active Oxygen Species. *Biochemistry* **1996**, *35*, 4584–4590.
68. Folk, D. S.; Franz, K. J. A Prochelator Activated by β-Secretase Inhibits Aβ Aggregation and Suppresses Copper-Induced Reactive Oxygen Species Formation. *J. Am. Chem. Soc.* **2010**, *132*, 4994–4995.
69. Mira, L.; Tereza Fernandez, M.; Santos, M.; Rocha, R.; Helena Florêncio, M.; Jennings, K. R. Interactions of Flavonoids with Iron and Copper Ions: A Mechanism for their Antioxidant Activity. *Free Radical Res.* **2002**, *36*, 1199–1208.
70. Besser, J. M.; Brumbaugh, W. G.; Ingersoll, C. G.; Ivey, C. D.; Kunz, J. L.; Kemble, N. E.; Schlekat, C. E.; Garman, E. R. Chronic Toxicity of Nickel-Spiked Freshwater Sediments: Variation in Toxicity among Eight Invertebrate Taxa and Eight Sediments. *Environ. Toxicol. Chem.* **2013**, 10.1002/etc.2271.
71. Chakrabarti, D. J.; Laughlin, D. E. The Cu-S (Copper-Sulfur) System. *Bull. Alloy Phase Diagrams* **1983**, *4*, 254–271.
72. Luther, G. W.; Theberge, S. M.; Rozan, T. F.; Rickard, D.; Rowlands, C. C.; Oldroyd, A. Aqueous Copper Sulfide Clusters as Intermediates During Copper Sulfide Formation. *Environ. Sci. Technol.* **2002**, *36*, 394–402.
73. Gautam, U.; Mukherjee, B. A Simple Synthesis and Characterization of CuS Nanocrystals. *Bull. Mater. Sci.* **2006**, *29*, 1–5.
74. Hoffmann, M. R.; Lim, B. C. Kinetics and Mechanism of the Oxidation of Sulfide by Oxygen: Catalysis by Homogeneous Metal-Phthalocyanine Complexes. *Environ. Sci. Technol.* **1979**, *13*, 1406–1414.
75. Hollmark, H. M.; Vegelius, J. R.; Kristiansen, P.; Werme, L.; Duda, L.-C. Exposure of Oxidized Copper Surfaces to Aqueous Na_2S Solution Studied with Soft X-Ray Spectroscopy. *J. Electrochem. Soc.* **2011**, *158*, C1–C5.
76. Raevskaya, A. E.; Stroyuk, A. L.; Kuchmii, S. Y.; Kryukov, A. I. Catalytic Activity of CuS Nanoparticles in Hydrosulfide Ions Air Oxidation. *J. Mol. Catal. A: Chem.* **2004**, *212*, 259–265.
77. Donner, E.; Howard, D. L.; Jonge, M. D. d.; Paterson, D.; Cheah, M. H.; Naidu, R.; Lombi, E. X-Ray Absorption and Micro X-Ray Fluorescence Spectroscopy Investigation of Copper and Zinc Speciation in Biosolids. *Environ. Sci. Technol.* **2011**, *45*, 7249–7257.
78. Lombi, E.; Donner, E.; Tavakkoli, E.; Turney, T. W.; Naidu, R.; Miller, B. W.; Scheckel, K. G. Fate of Zinc Oxide Nanoparticles During Anaerobic Digestion of Wastewater and Post-Treatment Processing of Sewage Sludge. *Environ. Sci. Technol.* **2012**, *46*, 9089–9096.
79. Limbach, L. K.; Wick, P.; Manser, P.; Grass, R. N.; Bruinink, A.; Stark, W. J. Exposure of Engineered Nanoparticles to Human Lung Epithelial Cells: Influence of Chemical Composition and Catalytic Activity on Oxidative Stress. *Environ. Sci. Technol.* **2007**, *41*, 4158–4163.
80. Jomova, K.; Valko, M. Advances in Metal-Induced Oxidative Stress and Human Disease. *Toxicology* **2011**, *283*, 65–87.
81. Li, M.; Zhu, L.; Lin, D. Toxicity of Zno Nanoparticles to *Escherichia coli*: Mechanism and the Influence of Medium Components. *Environ. Sci. Technol.* **2011**, *45*, 1977–1983.
82. VanWinkle, B. A.; D. M. B., K. L.; Malecki, J. M.; Gunter, K. K.; Evans, I. M.; Elder, A.; Finkelstein, J. N.; Oberdörster, G.; Gunter, T. E. Nanoparticle (NP) Uptake by Type I Alveolar Epithelial Cells and Their Oxidant Stress Response. *Nanotoxicology* **2009**, *3*, 307–318.